Regulation of dendritic spine growth through activity-dependent recruitment of the brain-enriched Na^+/H^+ exchanger NHE5

Graham H. Diering[a], Fergil Mills[b], Shernaz X. Bamji[b], and Masayuki Numata[a]
[a]Department of Biochemistry and Molecular Biology and [b]Department of Cellular and Physiological Sciences, University of British Columbia, Vancouver, BC, Canada V6T 1Z3

ABSTRACT **Subtle changes in cellular and extracellular pH within the physiological range have profound impacts on synaptic activities. However, the molecular mechanisms underlying local pH regulation at synapses and their influence on synaptic structures have not been elucidated. Dendritic spines undergo dynamic structural changes in response to neuronal activation, which contributes to induction and long-term maintenance of synaptic plasticity. Although previous studies have indicated the importance of cytoskeletal rearrangement, vesicular trafficking, cell signaling, and adhesion in this process, much less is known about the involvement of ion transporters. In this study we demonstrate that *N*-methyl-D-aspartate (NMDA) receptor activation causes recruitment of the brain-enriched Na^+/H^+ exchanger NHE5 from endosomes to the plasma membrane. Concomitantly, real-time imaging of green fluorescent protein–tagged NHE5 revealed that NMDA receptor activation triggers redistribution of NHE5 to the spine head. We further show that neuronal activation causes alkalinization of dendritic spines following the initial acidification, and suppression of NHE5 significantly retards the activity-induced alkalinization. Perturbation of NHE5 function induces spontaneous spine growth, which is reversed by inhibition of NMDA receptors. In contrast, overexpression of NHE5 inhibits spine growth in response to neuronal activity. We propose that NHE5 constrains activity-dependent dendritic spine growth via a novel, pH-based negative-feedback mechanism.**

Monitoring Editor
Paul Forscher
Yale University

Received: Jan 25, 2011
Revised: Mar 31, 2011
Accepted: Apr 27, 2011

INTRODUCTION

Many components of the synaptic machinery, such as voltage-gated calcium channels (VGCCs) and *N*-methyl-D-aspartate (NMDA) receptors, are known to be sensitive to changes in pH within the physiological range (Traynelis and Cull-Candy, 1990; Tang *et al.*, 1990; Klockner and Isenberg, 1994; Chen *et al.*, 1996; Tombaugh and Somjen, 1996; Chesler, 2003; Banke *et al.*, 2005). In addition, electrical activity in the CNS has been shown to elicit rapid pH changes in both intracellular and extracellular compartments. These localized acid–base transients in turn influence neural activity by a feedback onto pH-sensitive synaptic components (DeVries, 2001; Fedirko *et al.*, 2007; Makani and Chesler, 2007). Significant drops in extracellular pH observed during stroke and the following seizure activity have been shown to strongly inhibit synaptic transmission (Somjen, 1984; Siesjo *et al.*, 1985; Li and Siesjo, 1997; Chesler, 2003). However, the roles of subtler, localized pH changes that occur normally in the brain have not been fully investigated. Moreover, the specific molecules responsible for regulating synaptic pH have not been identified.

Excitatory synapses undergo long-lasting changes in synaptic strength such as long-term potentiation (LTP) and long-term depression (Malenka and Nicoll, 1999; Malenka and Bear, 2004; Kessels and Malinow, 2009). Most forms of LTP are initiated by activation of

This article was published online ahead of print in MBoC in Press (http://www.molbiolcell.org/cgi/doi/10.1091/mbc.E11-01-0066) on May 5, 2011.

Address correspondence to: Masayuki Numata (mnumata@mail.ubc.ca) or Shernaz X. Bamji (shernaz.bamji@ubc.ca).

Abbreviations used: AMPA, α-amino-3-hydroxyl-5-methyl-4-isoxazole-propionate; AP5, 2-amino-5-phosphonopentanoic acid; BCECF, 2′,7′-bis-(2-carboxyethyl)-5-(and-6)-carboxyfluorescein; DIV, days in vitro; EIPA, 5-(*N*-ethyl-*N*-isopropyl) amiloride; HA, hemagglutinin; HEPES, 4-(2-hydroxyethyl)-1-piperazineethanesulfonic acid; LTP, long-term potentiation; MAP, microtubule-associated protein; NHE, Na^+/H^+ exchanger; NMDA, *N*-methyl-D-aspartate; PSD95, postsynaptic density protein of 95 kDa; RACK1, receptor for active C-kinase; TTX, tetrodotoxin; VGAT, vesicular γ-amino butyric acid transporter; VGCC, voltage-gated Ca^{2+} channel; VGlut, vesicular glutamate transporter.

synaptic NMDA receptors (Malenka and Bear, 2004), followed by an increase in synaptic strength due to recruitment of postsynaptic α-amino-3-hydroxyl-5-methyl-4-isoxazole-propionate (AMPA) receptors (Shepherd and Huganir, 2007; Kessels and Malinow, 2009) and an increase in the number and size of dendritic spines, small protrusions of the dendrites on which excitatory postsynaptic compartments are localized (Engert and Bonhoeffer, 1999; Maletic-Savatic *et al.*, 1999; Matsuzaki *et al.*, 2004; Lang *et al.*, 2004). Due to the pH-sensitive nature of the NMDA receptor, local pH changes may influence the induction and maintenance of LTP (Velisek, 1998; Ronicke *et al.*, 2009).

Several studies have suggested that Na^+/H^+ exchange is the predominant pH-regulatory mode in isolated nerve terminals (Sauvaigo *et al.*, 1984; Nachshen and Drapeau, 1988). Na^+/H^+ exchange has also been implicated in the regulation of synaptic transmission at glutamatergic, GABAergic, and dopaminergic synapses (Trudeau *et al.*, 1999; Jang *et al.*, 2006; Rocha *et al.*, 2008; Dietrich and Morad, 2010). Mammals have nine isoforms of Na^+/H^+ exchanger (NHE1–9), of which NHE1 and NHE5 are highly expressed in the brain (Brett *et al.*, 2005). NHE5 mRNA is expressed almost exclusively in the brain, showing the most-restricted distribution of any NHE isoform (Attaphitaya *et al.*, 1999; Baird *et al.*, 1999). The restricted expression of NHE5 suggests that it may have a unique function in the brain. However, the physiological role of NHE5 and the tissue and subcellular distribution of NHE5 protein remain unknown.

We demonstrate that enhanced neuronal activity increases the localization of NHE5 to dendritic spines and increases spine pH. Overexpression of NHE5 blocks activity-induced spine outgrowth. Conversely, knockdown of NHE5, or expression of dominant-negative NHE5 mutant, results in exuberant spine outgrowth. We propose that NHE5 acts as a negative regulator of activity-dependent spine growth by regulating pH-sensitive synaptic proteins.

RESULTS

NHE5 is expressed in hippocampal neurons

Previous studies from other laboratories have shown robust NHE5 mRNA expression in neuron-rich structures such as the hippocampus and cerebral cortex (Attaphitaya *et al.*, 1999; Baird *et al.*, 1999). However, it is not known whether NHE5 protein is present in brain for potential function. To address this question, we generated a polyclonal antibody against a peptide corresponding to the first extracellular loop of rat NHE5. The specificity of this antibody was verified by Western blot and immunofluorescence microscopy (Supplemental Figure S1). Immunolabeling of mouse coronal brain sections revealed robust NHE5 protein expression in CA1–CA3 hippocampal pyramidal neurons (Figure 1, A, A′, and B), as well as within the stratum radiatum layer where CA3 neurons synapse onto CA1 pyramidal cells (Figure 1, A and A″). This result shows for the first time that NHE5 protein is expressed in neurons.

To examine the subcellular distribution of NHE5 in hippocampal neurons, primary hippocampal cultures were labeled with the anti-NHE5 antibody. NHE5 displayed a punctate staining pattern and was expressed in neurites positive for either microtubule-associated protein 2 (MAP2) or tau protein, suggesting that NHE5 is present in both dendrites and axons (unpublished data). NHE5 puncta often overlapped with the excitatory synapse markers vesicular glutamate transporter 1 (VGlut1) and postsynaptic density protein of 95 kDa (PSD95) (Figure 1C), and occasionally with the inhibitory synapse markers vesicular γ-amino butyric acid (GABA) transporter (VGAT) and gephyrin (Figure 1D). Threshold analysis of triple colocalization between NHE5 and presynaptic and postsynaptic markers revealed that 39.8% of excitatory synapses and 23.8% of inhibitory synapses were positive for NHE5. Although NHE5 is not a global component of synapses, these results suggest that at steady state, NHE5 is targeted to a subset of synapses.

NHE5 is recruited to the cell surface by synaptic activity

Ronicke and colleagues previously suggested a role of pH-regulatory proteins at excitatory synapses and LTP (Ronicke *et al.*, 2009). This finding led us to postulate that NHE5 might regulate excitatory synapse function, and therefore we primarily focus our attention on excitatory neurons in this study. In response to synaptic activity, synapses undergo extensive remodeling of membrane composition, which requires delivery of some membrane proteins from recycling endosomes in a Rab11-dependent pathway (Park *et al.*, 2004, 2006; Wang *et al.*, 2008). Given that NHE5 traffics between recycling endosomes and the plasma membrane via the Rab11 pathway (Diering *et al.*, 2009), we speculated that NHE5 localization to synapses and the plasma membrane might be regulated by synaptic activity. To test this possibility, we manipulated neuronal activity in culture by treating neurons at 12 d in vitro (12DIV) for 48 h with bicuculline (20 μM), which enhances neuronal activity by blocking inhibitory $GABA_A$ receptors (Curtis *et al.*, 1971), or tetrodotoxin (TTX, 1 μM), which suppresses neuronal activity by inhibiting voltage-gated Na^+ channels (Narahashi *et al.*, 1964). At 14DIV surface NHE5 levels were quantified following bicuculline or TTX treatment using a cell-surface biotinylation assay. Compared to untreated control neurons, surface NHE5 levels were significantly increased or decreased in bicuculline- or TTX-treated neurons, respectively (Figure 2, A and B). Alternatively, we enhanced synaptic activity in a more acute manner by using a previously described cocktail of glycine, bicuculline, and TTX (Lu *et al.*, 2001). This paradigm has been used in hippocampal slices to induce chemical LTP (Shahi *et al.*, 1993; Musleh *et al.*, 1997), and glycine is used routinely to acutely enhance activity in neuronal cultures through activation of NMDA receptors (Lu *et al.*, 2001; Park *et al.*, 2006). Compared to untreated cultures (14DIV), there was a marked increase in surface NHE5 in neurons treated with glycine (200 μM for 3 min). This increase was completely prevented by the NMDA-receptor inhibitor D-AP5 (100 μM) (Collingridge *et al.*, 1983; Figure 2, C and D). Recruitment of NHE5 to the cell surface occurred in a time-dependent manner beginning within 5 min following glycine treatment (Figure 2, E and F). Notably, this increase in recruitment of NHE5 to the cell surface following glycine treatment was specific, as no change in surface or total expression of NHE1 was observed following bicuculline, TTX, or glycine treatment (Figure 2, A–F). These results suggest that surface NHE5 abundance in neurons is bidirectionally regulated by neuronal activity in both a chronic and an acute manner.

NHE5 is delivered to synapses and dendritic spines following synaptic activity

Next, we used immunofluorescence microscopy to determine whether NHE5 targeting to synapses was also activity dependent. 14DIV hippocampal neurons were treated with 200 μM glycine or control solution for 3 min to enhance activity. At 45 min after glycine stimulation, neurons were fixed and NHE5 localization at excitatory synapses was assessed. We noted a significant increase in the number of excitatory synapses positive for NHE5 following glycine treatment (45.1 ± 4.7% control, 73.3 ± 2.2% glycine treated, $p < 0.01$, Student's *t* test; Supplemental Figure S2).

To determine whether the NHE5 recruited to synapses was inserted into the plasma membrane, we took advantage of the fact that the anti-NHE5 antibody raised against the first extracellular loop of

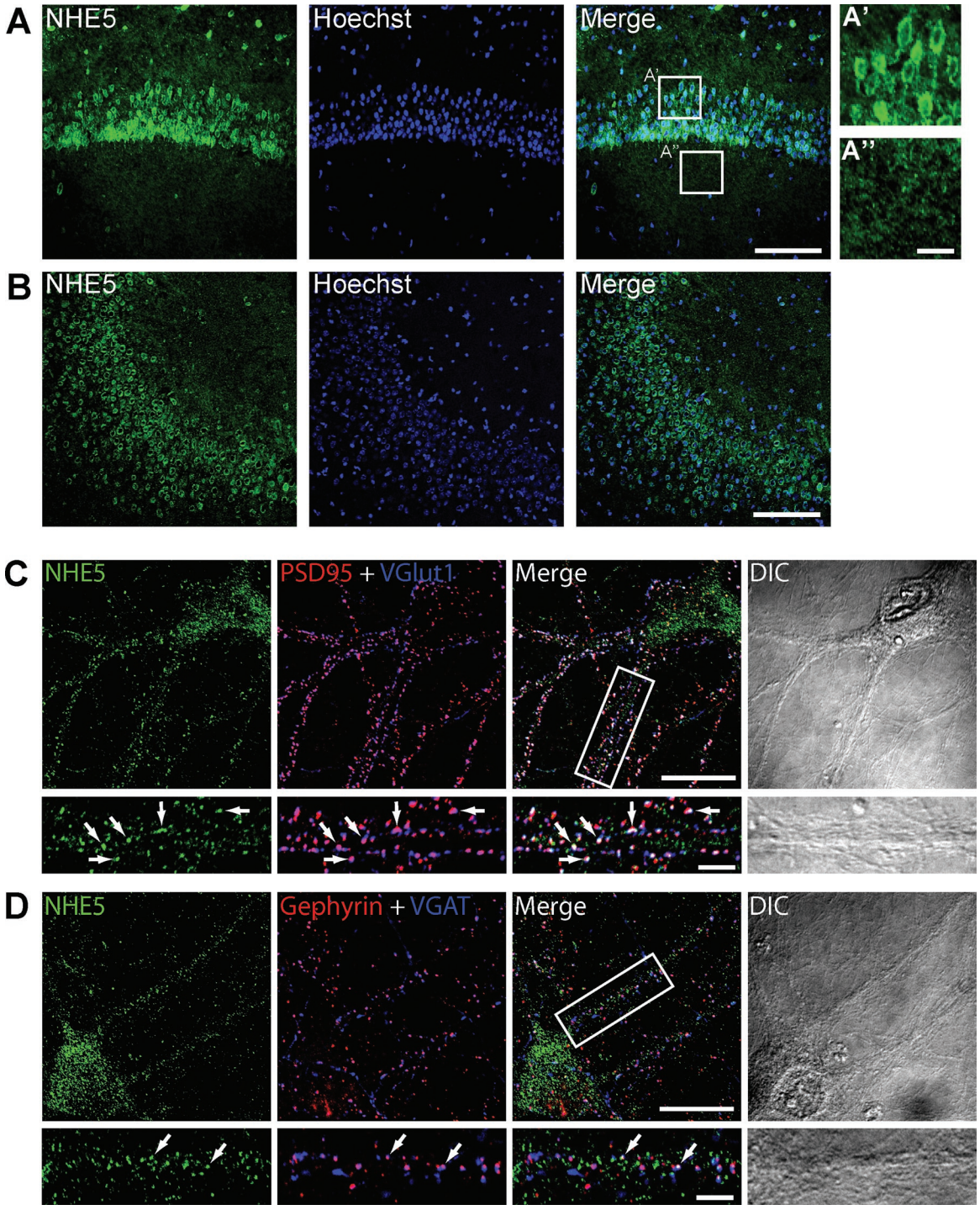

FIGURE 1: NHE5 is expressed in hippocampal neurons. (A, B) Confocal images of adult mouse brain coronal sections demonstrate NHE5 immunolabeling in CA1 pyramidal neurons of the hippocampus (A′) and stratum radiatum (A″) and hippocampus CA3 (B). Scale bar, 100 μm; inset 10 μm. (C, D) Confocal images of cultured rat hippocampal neurons immunolabeled for NHE5 and the excitatory presynaptic and postsynaptic markers VGlut1 and PSD95, respectively (C), or the inhibitory presynaptic and postsynaptic markers VGAT and gephyrin (D). Scale bar, 20 μm; inset, 5 μm. Arrows indicate regions of triple colocalization between NHE5 and synapse markers suggesting synaptic localization of NHE5.

NHE5 could specifically recognize surface NHE5 in fixed neurons by immunofluorescence microscopy under nonpermeabilized conditions. We found that very little NHE5 is present at the cell surface at steady state, and that surface NHE5 was almost exclusively localized to synapses, as shown by colocalization of surface NHE5 with PSD95 and VGlut1 (Figure 3A). Following glycine treatment, we noted a dramatic increase in the number and intensity of NHE5 puncta at the cell surface (Figure 3B). Similar to that observed at steady state, surface NHE5 was almost exclusively localized to synapses (Figure 3, A and B). Quantitative colocalization analysis revealed a significant increase in the number of synapses positive for surface NHE5 following glycine treatment compared with untreated cells (Figure 3C).

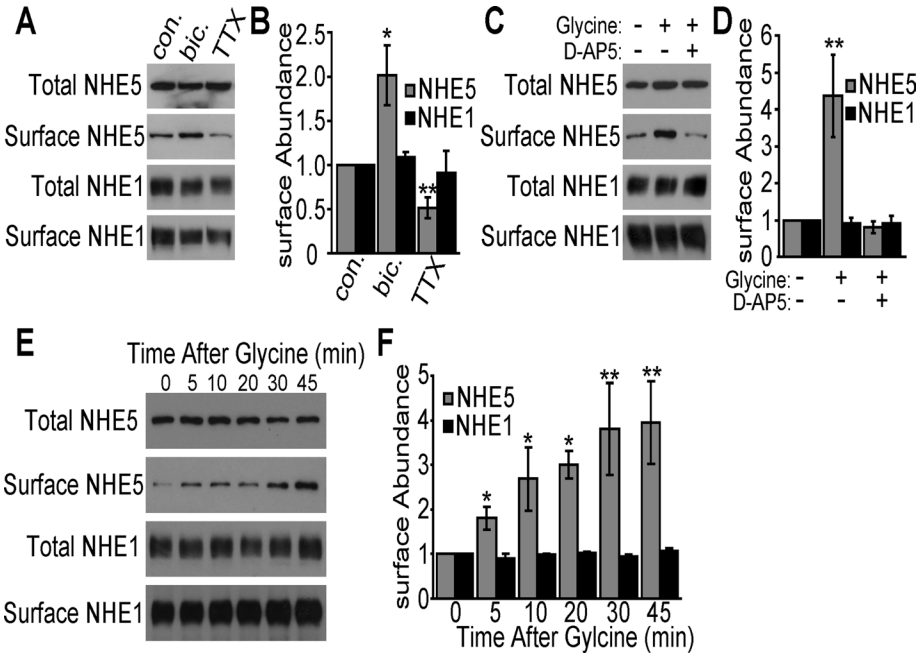

FIGURE 2: Activity-dependent targeting of NHE5 to the plasma membrane. (A) Cultured hippocampal neurons were left untreated (con.) or treated for 48 h with bicuculline (20 μM, bic.) or TTX (1 μM) to enhance or suppress network activity, respectively. Neurons were then surface biotinylated, and total and surface abundance of NHE5 and NHE1 were measured by Western blot. (B) Surface NHE1 and NHE5 from bicuculline- or TTX-treated neurons were normalized to untreated control lanes. (C) Cultured hippocampal neurons were treated with or without glycine (200 μM for 3 min) or D-AP5 (100 μM, 30-min pretreatment) followed by a 45-min chase. Neurons were then cell surface biotinylated. There is a dramatic increase in biotinylated surface NHE5, but not NHE1, following glycine treatment, and this increase could be blocked by D-AP5. (D) Surface NHE1 and NHE5 from glycine/D-AP5–treated neurons were normalized to untreated control lanes. (E) Cultured hippocampal neurons were treated with glycine (as in C) with a 0- to 45-min chase as indicated, followed by cell surface biotinylation. There is a time-dependent increase in biotinylated surface NHE5, but not NHE1, beginning 5 min following glycine treatment. (F) Surface NHE1 and NHE5 from glycine-treated neurons were normalized to untreated (0 min) control lanes. For all biotinylation experiments, there were three independent experiments from three separate cultures. *$p < 0.05$ and **$p < 0.01$, Student's *t* test.

To analyze the activity-dependent trafficking of NHE5 by live-cell imaging, cells were transfected with NHE5-GFP plus RFP as a cell fill. Although overexpressed NHE5-GFP exhibited much higher fluorescence in dendrites than endogenous NHE5 staining in dendrites, endogenous NHE5 staining showed a considerable overlap with NHE5-GFP (Supplemental Figure S3). Before glycine treatment, NHE5-GFP was distributed in the dendritic shaft, at the base of dendritic spines, in the spine neck, or in the spine head (Figure 3E). Following glycine treatment, NHE5-GFP present at the base of several spines was observed to traffic to the spine neck and then the spine head (Figure 3D). Quantification of the distribution of NHE5-GFP at spines revealed a time-dependent decrease in the proportion of spines that displayed NHE5-GFP at their base or neck and a concomitant increase in the proportion of spines that displayed NHE5-GFP in the spine head (Figure 3E). No change in the spine distribution of NHE5-GFP was seen during the same period in mock-glycine–treated neurons (Supplemental Figure S3). Together, these data suggest that NHE5 is recruited to postsynaptic spines and to the plasma membrane in an activity-dependent manner.

NHE5 is a negative regulator of dendritic spine growth

Dendritic spines undergo extensive remodeling in response to LTP-inducing stimuli (Engert and Bonhoeffer, 1999; Maletic-Savatic *et al.*, 1999; Matsuzaki *et al.*, 2004; Lang *et al.*, 2004). Given that NHE5 is recruited to dendritic spines on glycine stimulation, we hypothesized that NHE5 might regulate activity-induced dendritic spine growth. To address this, we first used a short-hairpin RNA (shRNA) approach to knock down NHE5. Three independent shRNA constructs (shA, B, and C) were used to deplete NHE5 levels and resulted in up to 80% knockdown of endogenous NHE5 (Supplemental Figure S4). NHE5 shRNA–expressing neurons exhibited a significant increase in the density of dendritic spines and a small but significant increase in average spine head width (Figure 4, A and B). Expression of shRNA-resistant human NHE5 rescued these effects, suggesting the spine phenotypes observed in these NHE5 shRNA–expressing cells are not due to off-target effects. To further define the role of NHE5 in the dendritic spine phenotype, we explored the use of a dominant-negative mutant. Mutation of a highly conserved glutamate in human NHE1 (E266) was shown to abolish its ion transport activity, and heterologous expression of this mutant caused dominant-negative effects (Hisamitsu *et al.*, 2006; Busco *et al.*, 2010). Mutation of the corresponding highly conserved glutamate 209 in human NHE5 to isoleucine completely abolished the ion transport activity of this protein without affecting protein stability or trafficking, and this mutant exerted a dominant-negative effect on NHE5 transporter activity (Supplemental Figure S5). Heterologous expression of the dominant-negative NHE5 significantly enhanced dendritic spine density and head width. Moreover, the expression of neither mutant NHE5 nor wild-type NHE1 rescued the spine growth effects following NHE5 knockdown by shRNA (Figure 4, A and B). Together these findings suggest that NHE5 is a negative regulator of dendritic spine growth and that this requires NHE5-specific transporter activity.

NMDA receptor activation is an important step leading to changes in dendritic spine morphology and number (Engert and Bonhoeffer, 1999; Maletic-Savatic *et al.*, 1999; Matsuzaki *et al.*, 2004; Lang *et al.*, 2004; Malenka and Bear, 2004). Because NMDA receptors are inhibited by an increase in extracellular protons (Tang *et al.*, 1990; Traynelis and Cull-Candy, 1990; Banke *et al.*, 2005), we postulated that NHE5 recruited to the spine surface during activity may act as a local proton source to regulate NMDA receptor activity via local Na^+/H^+ exchange. To test this possibility, we treated transfected neurons with or without the NMDA-receptor antagonist D-AP5 (100 μM) for 48 h. Of interest, D-AP5 treatment reversed the dendritic spine phenotypes caused by shRNA or dominant-negative NHE5 (Figure 5, A and B), indicating that NHE5 typically limits exuberant spine growth by constraining NMDA-receptor activity. NMDA-receptor activity is typically low at rest due to the Mg^{2+} ion block (Nowak *et al.*, 1984). However, recent studies have demonstrated signaling through NMDA receptors during spontaneous synaptic transmission (Sutton *et al.*, 2004, 2006; Jung *et al.*, 2008; Espinosa and Kavalali, 2009). Our findings suggest that abrogating NHE5 activity reduces a local proton

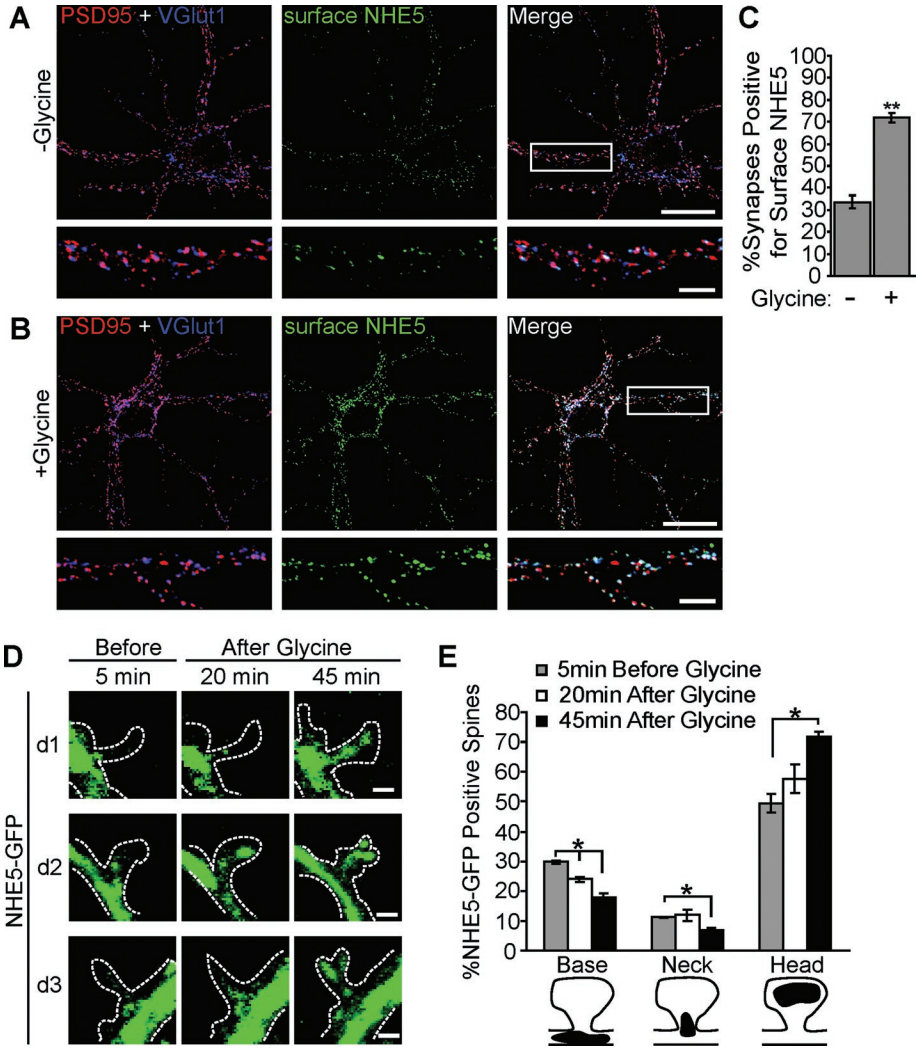

FIGURE 3: NHE5 is recruited to synapses and dendritic spines after glycine treatment. (A, B) Confocal images of hippocampal cultures left untreated (A) or treated with glycine for 3 min (B). Forty-five minutes after glycine treatment, cells were fixed and immunolabeled for surface NHE5 and the presynaptic and postsynaptic markers VGlut1 and PSD95, respectively. NHE5 was immunolabeled with the anti-NHE5 antibody under nonpermeable conditions, followed by permeabilization and immunolabeling of synaptic markers. Scale bar, 20 μm; inset, 5 μm. (C) Synapses were defined as regions of colocalization between PSD95 and VGlut1, and the percent of excitatory synapses positive for surface NHE5 was quantified. Data presented are the mean value (± SEM). There were 30 randomly selected fields from three separate cultures. **$p < 0.01$, Student's *t* test. (D) Time-lapse confocal images of 14DIV hippocampal neurons transfected with RFP plus NHE5-GFP and treated with glycine for 3 min. Three examples are provided (d1–d3). Dendrites and spines were visualized using the RFP cell fill and are depicted as a dashed outline for clarity. Before glycine treatment, NHE5-GFP is localized primarily at the base of spines in dendrites. At 20 and 45 min after glycine treatment, NHE5-GFP accumulates in spines in a time-dependent manner. Bar, 1 μm. (E) Localization of NHE5-GFP 5 min before or 20 and 45 min after glycine treatment. Spines were scored for content of NHE5-GFP at the base of the spine, in the spine neck, or in the spine head proper. There were up to 100 spines from each of three neurons from three separate cultures. *$p < 0.05$, Student's *t* test.

source at the synapse, increases the spontaneous NMDA receptor signaling, and leads to the NMDA-receptor–dependent exuberant spine growth.

NHE5 and activity-dependent spine growth

We next investigated the role of NHE5 in activity-induced spine growth. Hippocampal neurons were transfected with wild-type NHE5, dominant-negative mutant NHE5 (NHE5 E209I), or NHE5 shRNA. At 14DIV neurons were treated with glycine or control solution, and cells were fixed and analyzed 60 min later. In control GFP-expressing neurons, glycine treatment resulted in a significant increase in the density and head width of dendritic spines (Figure 6, A and B). This activity-induced enhancement of spine density and width was abolished in cells pretreated with the NMDA receptor antagonist D-AP5 (100 μM), confirming previous reports that the glycine treatment paradigm mediates its effects through activation of NMDA receptors (Lu *et al.*, 2001; Figure 6B). Expression of $NHE5_{HA}$-E209I or NHE5 shRNA significantly increased the basal dendritic spine density and increased the width slightly but in a statistically significant manner, and no further enhancement of spine density or head width was observed following glycine treatment, whereas wild-type NHE5 abolished activity-induced enhancement of spine density (Figure 6, A and B). These findings suggest that NHE5 activity is important for limiting activity-dependent formation of dendritic spines and that abrogating NHE5 function is sufficient to trigger spontaneous dendritic spine growth irrespective of neuronal activity.

Activity- and NHE5-dependent changes in dendritic spine pH

Our results demonstrating activity-dependent recruitment of NHE5 to dendritic spines and to the plasma membrane suggest that there may be an associated activity-dependent change in spine pH. To test this possibility, we initially attempted to determine pH of dendritic spines using a pH-sensitive variant of GFP (de4GFP). de4GFP is a dual-emission fluorophore that emits at both 510 and 460 nm, with emission at 510 nm increasing and emission at 460 nm decreasing as pH increases. Therefore, de4GFP could theoretically be used for ratiometric pH recordings (Hanson *et al.*, 2002; McAnaney *et al.*, 2002; Vilas *et al.*, 2009). However, we found that de4GFP emission at 460 nm was too faint to afford accurate pH measurement of dendritic spines. Therefore, to overcome this problem, we generated a chimera of pH-insensitive mCherry (Shaner *et al.*, 2005) fused to de4GFP (mCherry/de4GFP) for accurate ratiometric measurement of dendritic spine pH. A similar approach was successfully used with a fusion protein of mCherry and a pH-sensitive GFP variant SEpHluorin (Koivusalo *et al.*, 2010). In control experiments, we calibrated the fluorescence ratio of pH-insensitive mCherry and pH-sensitive de4GFP to cellular pH by expressing mCherry/de4GFP in Chinese hamster ovary cells and imaging these cells under pH-clamp conditions (Baxter and Church, 1996) using the protonophore nigericin (high

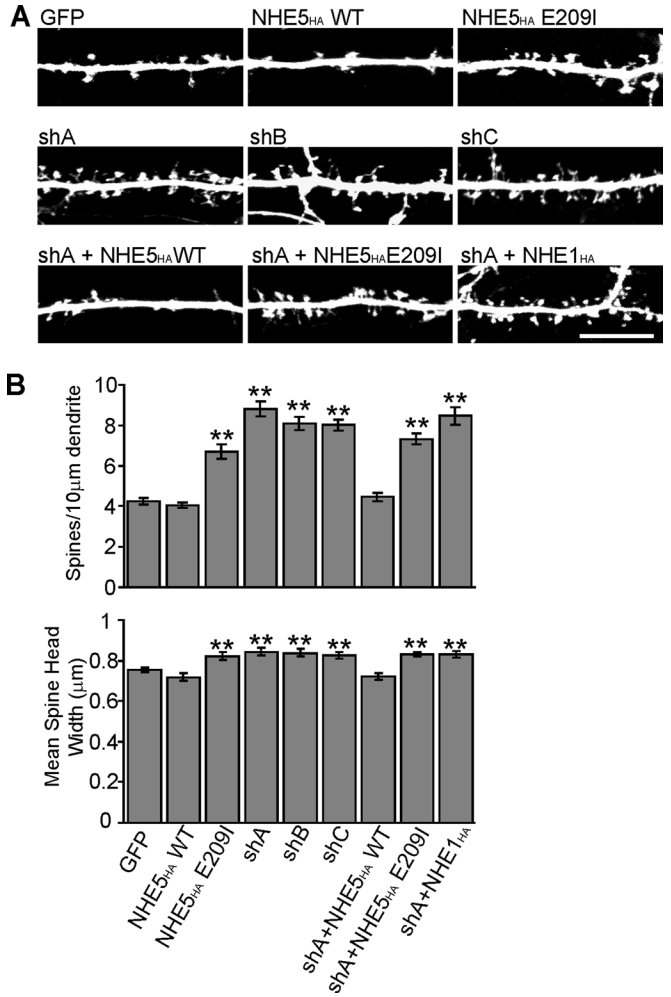

FIGURE 4: NHE5 is a negative regulator of spine density and head width. (A) Confocal images of 14DIV cultured hippocampal neurons transfected at 9DIV with GFP alone or together with HA-tagged human NHE5 wild-type ($NHE5_{HA}$ WT) or transport-deficient mutant ($NHE5_{HA}$ E209I), or shRNA constructs (shA–C). Scale bar, 10 μm. (B) The mean spine density and head width (± SEM) was measured in transfected neurons. There were 24–37 neurons per condition from three separate cultures. **Statistical significance, $p < 0.01$, compared with GFP-transfected control, Student's *t* test.

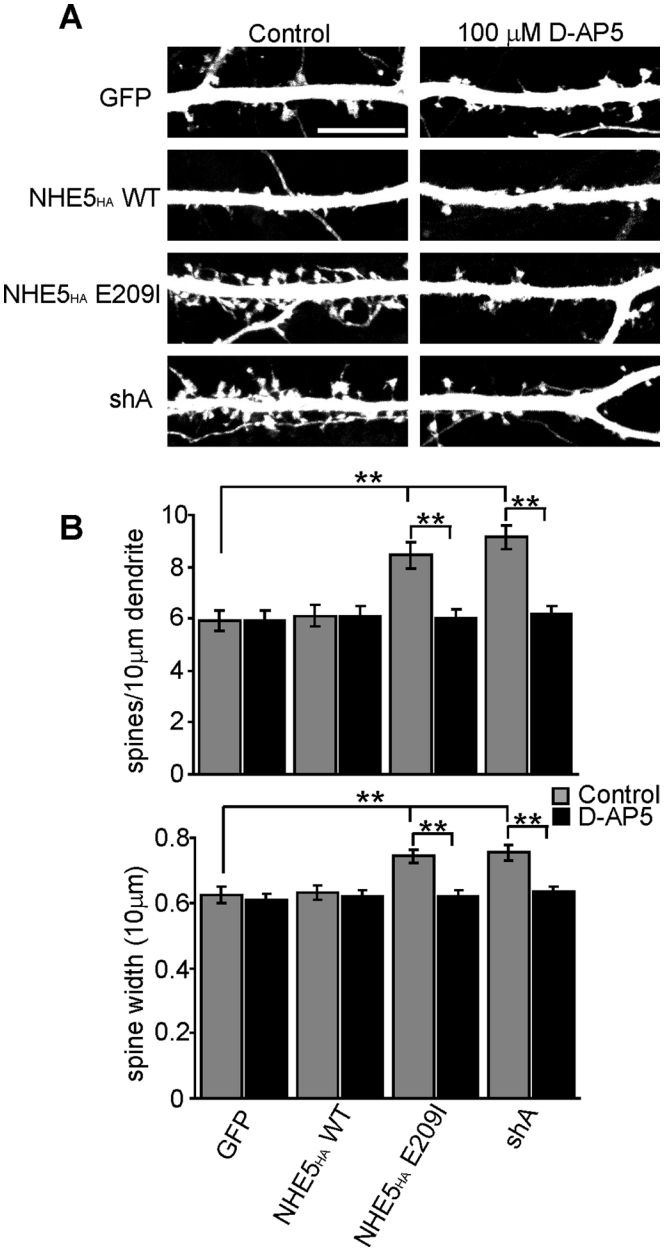

FIGURE 5: Spine growth associated with reduced NHE5 activity requires active NMDA receptors. (A) Confocal images of 14DIV cultured neurons transfected at 9DIV with GFP alone or together with the indicated construct. Transfected neurons were left untreated or treated with 100 μM D-AP5 (added to the culture medium) for 48 h before fixation at 14DIV. Scale bar, 10 μm. (B) The mean dendritic spine density and head width (± SEM) in untreated (gray bars) and D-AP5–treated neurons (black bars) was measured. There were 19–46 neurons per condition from three separate cultures. **$p < 0.01$, Student's *t* test.

K^+, 10 μM nigericin) (Figure 7A). We found a linear correlation between intracellular pH and background-subtracted mCherry/de4GFP fluorescence ratio within a pH range between 6.75 and 8.0 (Figure 7B). We then transfected neurons with mCherry/de-4GFP alone (control) or together with shRNA to knock down NHE5 (shA) and measured dendritic spine pH at rest before glycine treatment and with time after glycine treatment. The resting pH before glycine treatment was not significantly different between control and shA-transfected neurons. In control neurons, we noted an initial modest acidification of dendritic spines, followed by a time-dependent increase in dendritic spine pH beginning 5–10 min after glycine treatment that reached a new steady state 45–60 min after glycine treatment (Figure 7, C and D). This activity-induced alkalinization is consistent with the recruitment of NHE5 to the dendritic spine surface and subsequent export of spine protons to the extracellular space. A sustained alkaline shift of similar magnitude has been previously demonstrated in hippocampal neurons under other conditions (Smith *et al.*, 1998). In contrast, in NHE5 knockdown cells, the spine alkalinization was greatly attenuated following glycine treatment and returned to preglycine levels after 60 min (Figure 7, C and D). In mCherry/de4GFP–expressing neurons not treated with glycine there was no change in spine pH over a 60-min imaging period (unpublished data). Altogether, these results suggest that NHE5 is recruited to the dendritic spine membrane where NHE5 affects local pH following synaptic activity.

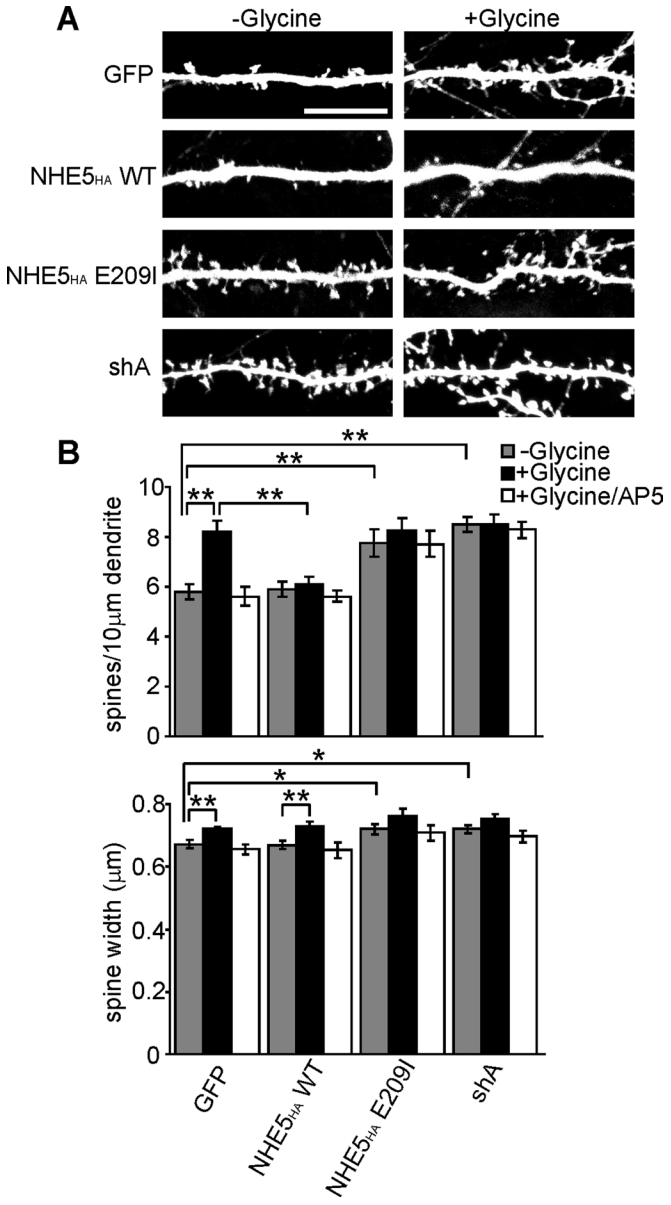

FIGURE 6: NHE5 modulates activity-induced increases in spine density and head width. (A) Confocal images of 14DIV cultured neurons transfected at 9DIV with GFP alone or together with the indicated construct. Neurons were either left untreated or treated with glycine for 3 min to enhance activity and imaged 60 min postglycine. As control, neurons were treated with D-AP5 (100 μM) for 30 min before and during glycine treatment. Scale bar, 10 μm. (B) The mean dendritic spine density and head width (± SEM) in untreated (gray bars), glycine-treated (black bars), and glycine/D-AP5–treated neurons (white bars) was measured. There were 17–28 neurons from three separate cultures. *$p < 0.05$ and **$p < 0.01$, Student's *t* test.

DISCUSSION

The synapse is made up from two principal components—the presynapse, where neurotransmitter-loaded synaptic vesicles are found, and the postsynapse, where neurotransmitter receptors are clustered opposite the vesicle release sites. These two structures are separated by a narrow space of approximately 20 nm, referred to as the synaptic cleft. Many components of the synaptic machinery found in the synaptic cleft are sensitive to changes in cleft pH, including VGCCs, AMPA receptors, kainate receptors, NMDA receptors, GABA receptors, type III metabotropic glutamate receptors, and acid-sensing ion channels, ion channels directly gated by protons (Traynelis and Cull-Candy, 1990; Tombaugh and Somjen, 1996; Krishek *et al.*, 1996; Ihle and Patneau, 2000; Mott *et al.*, 2003; Zha *et al.*, 2006; Levinthal *et al.*, 2009). The NMDA receptor, which is essential for many forms of synaptic plasticity, and VGCCs, which mediate Ca^{2+}-dependent release of synaptic vesicles, are particularly important to consider, as these proteins have an especially high proton sensitivity, with a pK_a of 7.3–7.5 and 7.1–7.3, respectively (Tang *et al.*, 1990; Traynelis and Cull-Candy, 1990; Klockner and Isenberg, 1994; Chen *et al.*, 1996; Tombaugh and Somjen, 1996; Banke *et al.*, 2005). Thus at resting pH close to 7.3 (Chesler, 2003), a tonic proton block exists that maintains NMDA receptor and VGCC activity to ~50%. This implies that any slight deviation in local pH should theoretically have a profound impact on synaptic transmission and synaptic plasticity. NMDA receptors have even been shown to contain a discrete proton-binding site, distinct from other ligand-binding sites (Banke *et al.*, 2005). On the basis of the abundance of pH-sensitive proteins within the narrow confines of the synaptic cleft, it is highly likely that localized control of cleft pH will play an important role in synaptic transmission. Indeed, localized pH shifts at the synapse have been demonstrated to feed back onto nearby pH-sensitive NMDA receptors and VGCCs (DeVries, 2001; Fedirko *et al.*, 2007; Makani and Chesler, 2007). However, the mechanisms that control local pH at the synapse and the identity of synaptic pH-regulating proteins have not been determined.

We show here that following glycine treatment to enhance synaptic activity, NHE5 is targeted to the cell surface and recruited to synapses, where it initiates a local pH change through Na^+/H^+ exchange. Furthermore, our data suggest that NHE5 is a negative regulator of activity-induced dendritic spine growth and that at rest NHE5 acts to suppress spontaneous spine growth. On the basis of these findings, we propose a model in which NHE5 is recruited to the synaptic plasma membrane in dendritic spines following synaptic activity (Figure 8). Once at the plasma membrane, NHE5 Na^+/H^+ exchanger activity results in alkalinization of the dendritic spine and concomitant acidification of the synaptic cleft. This local acidification may serve as an autocrine feedback mechanism that regulates pH-sensitive proteins at the postsynapse such as NMDA receptors and possibly also as a paracrine mechanism to regulate presynaptic pH-sensitive proteins such as VGCCs (Figure 8). The NMDA receptor is of particular interest, given its important role in dendritic spine remodeling (Engert and Bonhoeffer, 1999; Maletic-Savatic *et al.*, 1999; Lang *et al.*, 2004; Matsuzaki *et al.*, 2004). Overexpression of NHE5 may enhance the tonic proton block of the NMDA receptor, preventing activity-dependent formation of new spines. Conversely, reducing the local proton source by NHE5 knockdown or expression of a dominant-negative mutant may lead to hyperactivation of the NMDA receptor. This could effectively lower the threshold needed to induce LTP, such that spontaneous network activity is sufficient to drive dendritic spine expansion to an LTP-like state. Consistent with this idea, perturbation of NHE5 function led to a significant increase in dendritic spine density and width, which was not enhanced further by glycine treatment but was completely reversed by prolonged treatment with a chemical NMDA-receptor antagonist. In addition, spine alkalinization induced by glycine treatment was also prevented by knockdown of NHE5. Therefore, in our model, NHE5 acts as part of a negative-feedback loop to stabilize dendritic spine growth following NMDA receptor activation through a local pH shift at the synapse (Figure 8). Of interest, we showed previously that NHE5 directly interacts with the signaling scaffold molecule receptor for active C-kinase (RACK1) (Onishi *et al.*, 2007). RACK1 is also known

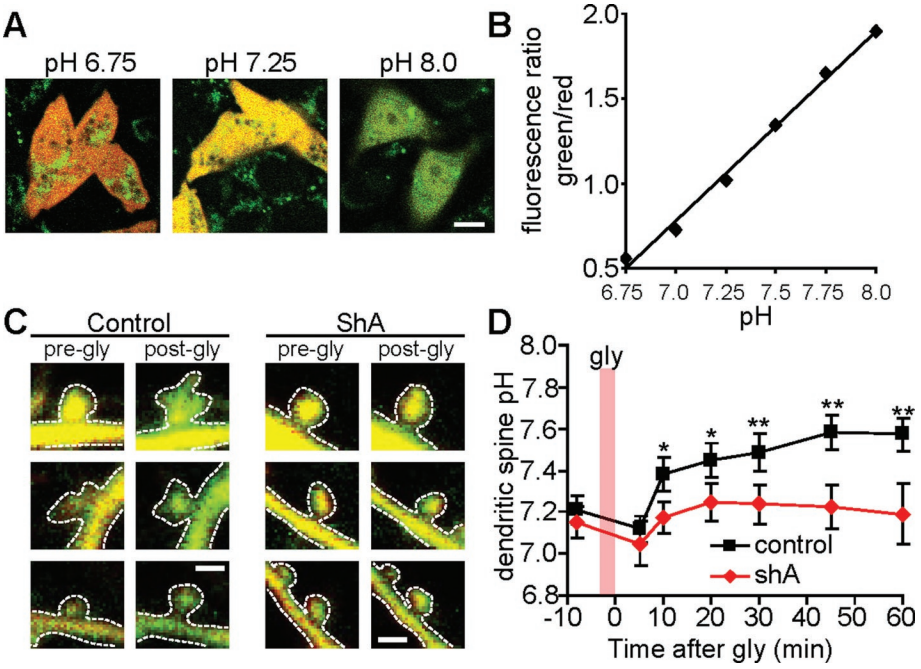

FIGURE 7: Activity-dependent changes in dendritic spine pH require functional NHE5. (A) Confocal images of Chinese hamster ovary cells transfected with mCherry/de4GFP and placed under pH-clamp conditions (high K^+, 10 μM nigericin). Sample images of merged green (de4GFP) and red (mCherry) fluorescence from cells under pH clamp—pH 6.75, 7.25, and 8.0—are shown. Scale bar, 10 μm. (B) Quantification of mCherry/de4GFP fluorescence ratio vs. intracellular pH from transfected Chinese hamster ovary cells pH clamped from pH 6.75 to 8.0. There were 140–330 cells for each pH value tested. (C) Confocal images of dendritic spines from neurons transfected with mCherry/de4GFP alone (control) or together with NHE5 shRNA (shA) 5 min before (pre-gly) or 60 min following glycine application (post-gly). Green (de4GFP) and red (mCherry) fluorescence signals were overlaid. An increase in green fluorescence indicates a pH shift in the alkaline direction. Three examples of each are shown. Scale bar, 1 μm. (D) Dendritic spine pH was monitored before glycine treatment and with time after glycine treatment. Up to 50 spines each were used from eight neurons per condition from three separate cultures. Statistical differences *$p < 0.05$ and **$p < 0.01$ from preglycine resting pH, Student's *t* test.

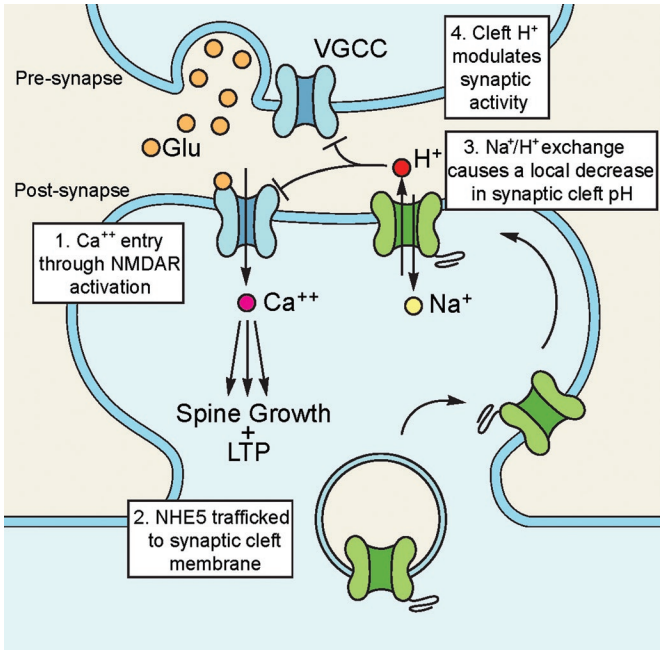

FIGURE 8: Proposed model for how NHE5 acts as a negative feedback molecule to limit activity-mediated spine growth.

to bind to the C-terminus of the NR2B subunit of the NMDA receptor (Yaka *et al.*, 2002). It is unknown how NHE5 is organized at the synapse at the molecular level, but one possibility is that RACK1 tethers NHE5 adjacent to the NMDA receptor through the NR2B subunit, making NHE5-transported protons a potent NMDA receptor inhibitor.

The primary focus of this study was to investigate the role of NHE5 at the postsynapse and in dendritic spines. However, due to the confined space of the synaptic cleft, it is possible that local pH shifts by NHE5 may feed back onto presynaptic molecules such as VGCCs in a similar manner as NMDA receptors. Furthermore, our immunocytochemical analyses suggest that NHE5 is also present in presynaptic compartments. Taken together, it is possible that local pH shifts by NHE5 may feed back onto presynaptic molecules such as VGCCs in a sophisticated manner. VGCCs are best known for their role in Ca^{2+}-dependent release of synaptic vesicles (Llinas *et al.*, 1982). Extracellular protons shift the activation voltage of VGCCs in the positive direction and reduce peak current, thereby decreasing synaptic vesicle release probability (Tombaugh and Somjen, 1996; DeVries, 2001). NHE5 inserted into the postsynapse membrane may serve to limit synaptic vesicle release from the presynapse through local acidification of the synaptic cleft. A similar proton-mediated feedback onto VGCCs has been demonstrated previously (DeVries, 2001). Thus it is interesting to speculate that reducing the local proton source by perturbation of NHE5 activity leads to higher vesicle release probability, which could act together with increased NMDA receptor activity to support the spontaneous dendritic spine growth that we observed.

Ronicke *et al.* (2009) showed that application of 5-(*N*-ethyl-*N*-isopropyl) amiloride (EIPA), an NHE-inhibitor drug, during tetanus induction of LTP in hippocampal CA1 neurons resulted in enhanced LTP, suggesting that NHE is a negative regulator of synapse plasticity. However, it is not clear which NHE isoform is responsible for this phenotype, as the high concentration of EIPA used in this study could inhibit all NHE activities across the plasma membrane in a nondiscriminatory manner. More recently, it was reported that NHE contributes to extracellular acidification of synapses and enhances GABAergic inhibitory signaling in cerebellar granule cells (Dietrich and Morad, 2010). Together with these studies, our current findings suggest that NHE5 is a negative regulator of synaptic activity. It will be an interesting future project to investigate targeting and function of NHE5 in inhibitory synapses.

To our knowledge, NHE5 is the first example of a synaptic pH-regulating ion transporter whose synapse and cell-surface targeting is controlled in an activity-dependent manner. We present evidence that NHE5 is a novel regulatory molecule involved in synaptic plasticity and add to a growing body of evidence supporting an important role for protons in synaptic transmission. As several components of the synaptic machinery are proton sensitive, local pH regulation at the synapse and NHE5

activity may affect multiple aspects of synapse physiology and warrants continued investigation.

MATERIALS AND METHODS

Antibodies. Rabbit polyclonal anti-NHE5 antibodies were raised against the epitope EEPTQEPGPLGEPP from rat NHE5 (amino acid residues 21–34), corresponding to the first extracellular loop of NHE5, and affinity purified (GenScript, Piscataway, NJ). The following additional primary antibodies were used: mouse monoclonal anti-Tau (Millipore, Billerica, MA), guinea pig polyclonal anti-VGlut1 (Millipore), mouse monoclonal anti-NHE1 (BD Biosciences, San Jose, CA), mouse monoclonal anti-MAP2 (Sigma, Oakville, ON, Canada), mouse monoclonal anti–α- and β-tubulin (Sigma), rabbit polyclonal anti-actin (Sigma), guinea pig polyclonal anti-VGAT (Synaptic Systems, Göttingen, Germany), mouse monoclonal anti-gephyrin (Synaptic Systems), mouse monoclonal anti-GFP (Roche, Mississauga, ON, Canada), mouse monoclonal anti-hemagglutinin (HA) (Covance, Princeton, NJ), and mouse monoclonal anti-PSD95 (Abcam, San Francisco, CA). The following secondary antibodies were used: Alexa Fluor 488– or Alexa Fluor 568–conjugated goat anti-rabbit, Alexa Fluor 568– or Alexa Fluor 647–conjugated goat anti-mouse (Molecular Probes, Eugene, OR), Cy5-conjugated donkey anti–guinea pig (Jackson ImmunoResearch, West Grove, PA), and horseradish peroxidase–conjugated goat anti–rabbit and goat anti–mouse secondary antibodies (Jackson ImmunoResearch).

RNAi constructs and recombinant DNAs. Human NHE5 cDNA was cloned previously (Baird *et al.*, 1999). HA-tagged human NHE5 was produced previously by introducing an artificial *Not*I restriction endonuclease site into the coding sequence corresponding to leucine 36 (contained in the first predicted exomembrane loop), followed by insertion of triple HA epitope (Szaszi *et al.*, 2002). The E209I variant of NHE5 was produced by site-directed mutagenesis using QuikChange Mutagenesis Kit (Stratagene, La Jolla, CA) using human $NHE5_{HA}$ as a template. EGFP coding sequence flanked by *Not*I restriction endonuclease sites was amplified by PCR and then ligated into the artificial *Not*I site introduced into NHE5. The expected final protein product contains the full-length NHE5 with internal GFP located in the first exoplasmic loop. For short-hairpin RNA (shRNA A, B or C) constructs targeting rat NHE5 the following complementary synthetic oligonucleotides were used, 5′-GATCCC**GTTTGCTCTTGGTGAAACAGATGTTA**TTGATATCCG**TAACATCTGTTTCACCAAGAGCAAA**TTTTTTCCAAA-3′ (sense) and 5′-AGCTTTTGGAAAAAA**TTTGCTCTTGGTGAAACAGATGTTA**CGGATATCAA**TAACATCTGTTTCACCAAGAGCAAA**CGG-3′ (antisense, shRNA A); 5′-GATCCC**ATAGTGGTGGCCACAAAGTAGTCCT**TTGATATCCG-**AGGACTATTTGTGGCCACCACTAT**TTTTTTCCAAA-3′ (sense) and 5′-AGCTTTTGGAAAAAA**ATAGTGGTGGCCACAAAGTAGTCCT**-CGGATATCAA**AGGACTACTTTGTGGCCACCACTAT**GG-3′ (antisense, shRNA B); 5′-GATCCC**GTTTGTGGTAATCACTCCTCTTCACC**TTGATATCCG**GGTGAAGAGGAGTGATTACCACAAA**TTTTTTCCAAA-3′ (sense) and 5′-AGCTTTTGGAAAAAA **TTTGTGGTAATCACTCCTCTTCACC**CGGATATCAA**GGTGAAGAGGAGTGATTACCACAAA**CGG-3′ (antisense, shRNA C). Boldface type indicates sequences targeting rat NHE5. When annealed, duplexes contain 5′ and 3′ overhangs, which allowed cloning into the multicloning site in pRNAT-H1 vector (Stratagene).

Neuronal cell culture. Hippocampi from E18 rats were prepared as previously described (Xie *et al.*, 2000) and plated at a density of 130 cells/mm^2 on poly-L-lysine–coated coverslips for immunohistochemistry or plated at a density of 260 cells/mm^2 on 35-mm, polyethylenimine-coated, plastic culture dishes for Western analysis. For all analyses, neurons were transfected using Lipofectamine 2000 (Invitrogen Canada, Burlington, ON, Canada) at 9 DIV and imaged at 14 DIV.

Immunohistochemistry

Brain sections. Adult mice (P40–P60) were anesthetized by interperioteneal injection of 150 mg/kg ketamine and 15 mg/kg xylazine and transcardially perfused with ice-cold phosphate-buffered saline (PBS) (pH 7.4), followed by 4% paraformaldehyde (PFA) in PBS. The brains were quickly removed and postfixed in 4% PFA for 1 h before going through a series of sucrose-PBS solutions (10–30%). Whole brains were embedded in Tissue-Tek (Sakura Finetek, Torrance, CA), frozen in dry ice, and stored at −80°C. A cryostat (Micron Instruments, San Marcos, CA) was used to cut 20-μm-thick coronal sections. For immunohistochemistry, sections were permeabilized in 0.1% Triton-X for 30 min, blocked in 4% goat serum for 1 h at room temperature, and incubated with PBS containing 1% goat serum and anti-NHE5 antibody overnight at 4°C. Following washes with PBS, sections were then incubated with goat anti–rabbit Alexa Fluor 488–conjugated secondary antibody in PBS containing 1% goat serum for 1 h at room temperature.

Hippocampal neurons. Neurons were fixed by incubation with 4% PFA in PBS for 10 min at room temperature and then permeabilized with 0.1% Triton X-100 in PBS for 10 min at room temperature. Alternatively, cells were fixed/permeabilized by incubation with prechilled methanol at −20°C for 5 min. Cells were blocked by incubation with 10% goat serum in PBS for 1 h at room temperature, followed by incubation with primary antibodies in PBS containing 1% goat serum overnight at 4°C and fluorescently labeled secondary antibodies for 1 h at room temperature.

For experiments examining NHE5 surface expression, cells were fixed with 4% PFA blocked by incubation with 10% goat serum in PBS for 30 min followed by incubation with rabbit anti-NHE5 antibody in PBS containing 1% goat serum for 2 h at room temperature. Cells were then permeabilized with 0.1% Triton X-100, incubated overnight at 4°C with mouse anti-PSD95 and guinea pig anti-VGlut1 in PBS containing 1% goat serum, followed by incubation with Alexa 488–conjugated goat anti–rabbit, Alexa 568–conjugated goat anti–mouse, and Cy5-conjugated donkey anti–guinea pig secondary antibodies.

Glycine and drug treatment. Cultured hippocampal neurons were incubated in chemical LTP buffer (140 mM NaCl, 5 mM KCl, 1.5 mM $CaCl_2$, 25 mM 4-(2-hydroxyethyl)-1-piperazineethanesulfonic acid [HEPES], pH 7.4, 33 mM glucose, 500 nM TTX, and 20 μM bicuculline) for 30 min at 37°C. Neurons were then treated with chemical LTP buffer containing 200 μM glycine for 3 min at 37°C, followed by a return to buffer without glycine for the remainder of the experiment. Control cells were left in TTX/bicuculline solution without glycine. In some experiments, D-AP5 (100 μM) was added to the chemical LTP buffer during the 30-min pretreatment and 3-min glycine treatment steps. For chronic activity manipulations bicuculline (20 μM) or TTX (1 μM) was added to the culture medium for 48 h.

Biotin labeling and Western blot analysis. Neurons treated with glycine, bicuculline, or TTX for the indicated times were rinsed with ice-cold PBSCM (PBS containing 1 mM $MgCl_2$ and 0.1 mM $CaCl_2$, pH 8.0) and then incubated with a protein-reactive

biotinylation reagent (NHS-SS-Biotin [Thermo Scientific, Hudson, NH], 0.5 mg/ml in PBSCM) for 30 min at 4°C to label surface proteins, and excess biotinylation reagent was quenched by incubation with PBSCM containing 20 mM glycine. Equal amounts of cell lysates from each sample were incubated overnight at 4°C with NeutrAvidin agarose beads (Thermo Scientific). Proteins eluted from the beads were resolved by SDS–PAGE and detected by Western blot using anti-NHE5 or anti-NHE1 antibodies. Ten percent of the total whole-cell lysate not subjected to NeutrAvidin beads was also visualized by Western blot.

Image analysis and quantification

Quantification of synapse localization. Cells were immunolabeled using NHE5, VGlut1 and PSD95, or VGAT and gephyrin antibodies. Images were analyzed using ImageJ software (National Institutes of Health, Bethesda, MD) and a colocalization plug-in from the ImageJ website (http://rsb.info.nih.gov/ij/plugins/colocalization.html). Synapses were first identified as regions of colocalization greater than 10 pixels in size between presynaptic and postsynaptic markers: Vglut1 (threshold 1165) and PSD95 (threshold 1290) for excitatory synapses, or VGAT (threshold 765) and gephyrin (threshold 790) for inhibitory synapses. Thresholding levels were held constant between samples and experiments, randomly selected fields were imaged, and all the puncta were examined in a field. These regions of colocalization between presynaptic and postsynaptic markers were used to create a "mask," and regions greater than five pixels where NHE5 puncta overlapped with the mask were considered synapses positive for NHE5. Numbers of synapses positive for NHE5 were expressed as a percentage of the total number of synapses identified, quantified using the same threshold and size criteria. The mean numbers of colocalized synaptic puncta quantified from 30 or more fields in each treatment group were analyzed for statistical significance using Student's *t* test. On average, >130 excitatory synapses were scored per field (4000–7000 total excitatory synapses analyzed), and 70 inhibitory synapses were scored per field (2200 total).

Dendritic spine measurement. For all experiments examining spine number and morphology a GFP cell fill was used. Serial Z-section confocal images were compiled into a single image. Regions of dendrite within 100 µm from the cell body where dendritic spines were clearly visible (without excessive crossing of multiple dendrites or axons) were imaged. All spines on selected dendrite segments were measured and included in our analysis. Spines were identified as protrusions from the dendrite shaft <3 µm in length with or without a head or a discernible neck, that is, stubby spines. The density and width of spines were measured using ImageJ software. Statistical analysis and graph plotting were performed using Excel software (Microsoft, Redmond, WA). For the quantification of Figures 4B, 5B, and 6B, 3500–8000 µm of dendrite from 17–46 neurons per condition was analyzed. The n values correspond to the number of neurons analyzed.

Quantification of NHE5-GFP localization. Individual spines were first identified from the RFP cell fill and then manually scored for the presence of NHE5-GFP either contained within the spine or within 1 µm of the spine base. NHE5-GFP location relative to spines was categorized according to the presence of NHE5-GFP at the base of the spine (in the dendritic shaft within 1 µm of the spine base), in the spine neck (between the spine base and spine head), or in the spine head (at the spine tip) as illustrated in Figure 3E. Spines containing NHE5-GFP in the head or neck and extending to the spine base were counted as positive for spine head or neck and not as spine base.

Monitoring dendritic spine pH using the ratiometric mCherry/de4GFP fusion. The cDNA encoding mCherry was obtained from AddGene (Cambridge, MA) and used as a template to for PCR. *Hin*dIII and *Bam*HI sites were introduced to the 5′ and 3′ ends of the coding region of mCherry, respectively, by PCR and ligated into the corresponding sites of the pde4GFP-N1 vector (Vilas *et al*., 2009) in frame with de4GFP. Hippocampal neurons, grown on gridded glass-bottom dishes (MatTek, Ashland, MA), were transfected with mCherry/de4GFP fusion alone or together with NHE5 shRNA A. The de4GFP (pH-sensitive) and mCherry (pH-insensitive) fluorescence was captured using an Olympus (Center Valley, PA) FluoView confocal microscope by excitation with a 488- or 543-nm laser, respectively. To calibrate mCherry/de4GFP fluorescence ratio to pH, the high–[K+]/nigericin technique was used (Chaillet and Boron, 1985; Baxter and Church, 1996). In the calibration experiments, fluorescence intensity of de4GFP displayed a sigmoidal relationship to pH between pH 5.0 and 9.0, and pK_a was calculated to be 7.45, similar to the previously reported value (Hanson *et al*., 2002). Between pH 6.75 and 8.0, the relationship between pH and mCherry/de4GFP fluorescence ratio was linear (Vilas *et al*., 2009). Experimentally measured ratios for each spine were converted to pH using the linear relationship between fluorescence ratio and pH determined in mCherry/de4GFP–transfected Chinese hamster ovary cells under pH clamp.

Supplementary materials and methods

Cell lines. Chinese hamster ovary, AP-1, and AP-1–based cell lines were maintained in α-MEM with 10% fetal bovine serum (FBS), and PC12 and PC12 cells stably expressing NHE5 shRNA were maintained in DMEM supplemented with 5% FBS and 10% horse serum. AP-1 cells are an NHE-deficient cell line derived from Chinese hamster ovary cells produced previously by chemical mutagenesis (Rotin and Grinstein, 1989). AP-1 cells stably expressing HA-tagged NHE5 or NHE1 were produced previously (Szaszi *et al*., 2002). AP-1 cells expressing HA-tagged NHE5 E209I were produced by transfecting parental AP-1 cells with pcDNA3 containing $NHE5_{HA}$-E209I, using the conventional calcium phosphate method. Stable transfectants were selected in growth media containing G418 (200 µg/ml), and individual clones were screened by Western blot and immunofluorescence microscopy using mouse anti-HA antibody. PC12 cells stably expressing NHE5 shRNA (A, B, or C) were established in the same way.

NHE activity assay. Cells were loaded with the pH-sensitive dye 2′,7′-bis-(2-carboxyethyl)-5-(and-6)-carboxyfluorescein (BCECF) by incubation with 2 µM BCECF acetoxymethyl ester in NaCl-saline solution (130 mM NaCl, 5 mM KCl, 1 mM $MgCl_2$, 2 mM $CaCl_2$, 5 mM glucose, and 20 mM HEPES-NaOH, pH 7.4) for 10 min at room temperature. Coverslips with cells attached were then mounted in a temperature-controlled recording chamber filled with NaCl-saline solution, placed on the microscope stage, and superfused at 2 ml/min with NaCl-saline solution (without dye) at 34°C for the remainder of the experiment. The dual excitation ratio method was used to estimate pH_i with a fluorescence ratio imaging system (Atto Biosciences, Rockville, MD) as described previously (Baxter and Church, 1996). The high–[K^+]/nigericin technique was used to convert background-corrected BCECF emission intensity ratios into pH_i values (Rotin and Grinstein, 1989; Baxter and Church, 1996). Intracellular acid loads were imposed by exposing the cells for 2 min

to NH_4^+-choline solution containing 50 mM NH_4Cl followed by washout with Na^+-free solution containing equimolar choline chloride. Na^+/H^+ exchange was induced by the return to NaCl-saline solution. The recovery of pH_i following an NH_4^+ prepulse was fitted to a single-exponential function, and the first derivative of this function was used to determine the rate of change of pH_i (dpH_i/dt) at 0.05 pH_i unit increments from the point of maximum acidification (Baxter and Church, 1996). Proton efflux was calculated by multiplying the measured dpH_i/dt at a given pH_i value by the intrinsic intracellular buffering capacity (β_i) at the same pH_i value as determined previously (Diering *et al.*, 2009).

ACKNOWLEDGMENTS

We thank Joseph Casey (University of Alberta, Edmonton, AB, Canada) for kindly sharing the pH-sensitive GFP variant de4GFP. This work is supported by Natural Sciences and Engineering Research Council of Canada discovery grants to M.N. and Canadian Institutes of Health Research operating grants to S.X.B. G.H.D. is a recipient of a Michael Smith Foundation for Health Research Junior Graduate Studentship and Natural Sciences and Engineering Research Council of Canada Alexander Graham Bell Canada Graduate Scholarships M and D. F.M. is a recipient of a Michael Smith Foundation for Health Research Junior Graduate Studentship and Canadian Institutes of Health Research Frederick Banting and Charles Best Canada Graduate Scholarship D.

REFERENCES

Attaphitaya S, Park K, Melvin JE (1999). Molecular cloning and functional expression of a rat Na^+/H^+ exchanger (NHE5) highly expressed in brain. J Biol Chem 274, 4383–4388.

Baird NR, Orlowski J, Szabo EZ, Zaun HC, Schultheis PJ, Menon AG, Shull GE (1999). Molecular cloning, genomic organization, and functional expression of Na^+/H^+ exchanger isoform 5 (NHE5) from human brain. J Biol Chem 274, 4377–4382.

Banke TG, Dravid SM, Traynelis SF (2005). Protons trap NR1/NR2B NMDA receptors in a nonconducting state. J Neurosci 25, 42–51.

Baxter KA, Church J (1996). Characterization of acid extrusion mechanisms in cultured fetal rat hippocampal neurones. J Physiol 493, 457–470.

Brett CL, Donowitz M, Rao R (2005). Evolutionary origins of eukaryotic sodium/proton exchangers. Am J Physiol 288, C223–39.

Busco G *et al.* (2010). NHE1 promotes invadopodial ECM proteolysis through acidification of the peri-invadopodial space. FASEB J 24, 3903–3915.

Chaillet JR, Boron WF (1985). Intracellular calibration of a pH-sensitive dye in isolated, perfused salamander tubules. J Gen Physiol 86, 765–794.

Chen XH, Bezprozvanny I, Tsien RW (1996). Molecular basis of proton block of L-type Ca^{2+} channels. J Gen Physiol 108, 363–374.

Chesler M (2003). Regulation and modulation of pH in the brain. Physiol Rev 83, 1183–1221.

Collingridge GL, Kehl SJ, McKlennan H (1983). The antagonism of amino acid-induced excitations of rat hippocampal CA1 neurones in vitro. J Physiol 334, 19–31.

Curtis DR, Duggan AW, Felix D, Johnston GA (1971). Bicuculline, an antagonist of GABA and synaptic inhibition in the spinal cord of the cat. Brain Res 32, 69–96.

DeVries SH (2001). Exocytosed protons feedback to suppress the Ca^{2+} current in mammalian cone photoreceptors. Neuron 32, 1107–1117.

Diering GH, Church J, Numata M (2009). Secretory carrier membrane protein 2 regulates cell-surface targeting of brain-enriched Na^+/H^+ exchanger NHE5. J Biol Chem 284, 13892–13903.

Dietrich CJ, Morad M (2010). Synaptic acidification enhances $GABA_A$ signalling. J Neurosci 30, 16044–16052.

Engert F, Bonhoeffer T (1999). Dendritic spine changes associated with hippocampal long-term synaptic plasticity. Nature 399, 66–70.

Espinosa F, Kavalali ET (2009). NMDA receptor activation by spontaneous glutamatergic neurotransmission. J Neurophysiol 101, 2290–2296.

Fedirko N, Avshalumov M, Rice ME, Chesler M (2007). Regulation of postsynaptic Ca^{2+} influx in hippocampal CA1 pyramidal neurons via extracellular carbonic anhydrase. J Neurosci 27, 1167–1175.

Hanson GT, McAnaney TB, Park ES, Rendell ME, Yarbrough DK, Chu S, Xi L, Boxer SG, Montrose MH, Remington SJ (2002). Green fluorescent protein variants as ratiometric dual emission pH sensors. 1. structural characterization and preliminary application. Biochemistry 41, 15477–15488.

Hisamitsu T, Ben Ammar Y, Nakamura TY, Wakabayashi S (2006). Dimerization is crucial for the function of the Na^+/H^+ exchanger NHE1. Biochemistry 45, 13346–13355.

Ihle EC, Patneau DK (2000). Modulation of alpha-amino-3-hydroxy-5-methyl-4-isoxazolepropionic acid receptor desensitization by extracellular protons. Mol Pharmacol 58, 1204–1212.

Jang IS, Brodwick MS, Wang ZM, Jeong HJ, Choi BJ, Akaike N (2006). The Na^+/H^+ exchanger is a major pH regulator in GABAergic presynaptic nerve terminals synapsing onto rat CA3 pyramidal neurons. J Neurochem 99, 1224–1236.

Jung SC, Kim J, Hoffman DA (2008). Rapid, bidirectional remodeling of synaptic NMDA receptor subunit composition by A-type K^+ channel activity in hippocampal CA1 pyramidal neurons. Neuron 60, 657–671.

Kessels HW, Malinow R (2009). Synaptic AMPA receptor plasticity and behavior. Neuron 61, 340–350.

Klockner U, Isenberg G (1994). Calcium channel current of vascular smooth muscle cells: extracellular protons modulate gating and single channel conductance. J Gen Physiol 103, 665–678.

Koivusalo M, Welch C, Hayashi H, Scott CC, Kim M, Alexander T, Touret N, Hahn KM, Grinstein S (2010). Amiloride inhibits macropinocytosis by lowering submembranous pH and preventing Rac1 and Cdc42 signaling. J Cell Biol 188, 547–563 [correction published in J Cell Biol (2010). 189, 385].

Krishek BJ, Amato A, Connolly CN, Moss SJ, Smart TG (1996). Proton sensitivity of the GABA(A) receptor is associated with the receptor subunit composition. J Physiol 492, 431–443.

Lang C, Barco A, Zablow L, Kandel ER, Siegelbaum SA, Zakharenko SS (2004). Transient expansion of synaptically connected dendritic spines upon induction of hippocampal long-term potentiation. Proc Natl Acad Sci USA 101, 16665–16670.

Levinthal C, Barkdull L, Jacobson P, Storjohann L, Van Wagenen BC, Stormann TM, Hammerland LG (2009). Modulation of group III metabotropic glutamate receptors by hydrogen ions. Pharmacology 83, 88–94.

Li PA, Siesjo BK (1997). Role of hyperglycaemia-related acidosis in ischaemic brain damage. Acta Physiol Scand 161, 567–580.

Llinas R, Sugimori M, Simon SM (1982). Transmission by presynaptic spike-like depolarization in the squid giant synapse. Proc Natl Acad Sci USA 79, 2415–2419.

Lu W, Man H, Ju W, Trimble WS, MacDonald JF, Wang YT (2001). Activation of synaptic NMDA receptors induces membrane insertion of new AMPA receptors and LTP in cultured hippocampal neurons. Neuron 29, 243–254.

Makani S, Chesler M (2007). Endogenous alkaline transients boost postsynaptic NMDA receptor responses in hippocampal CA1 pyramidal neurons. J Neurosci 27, 7438–7446.

Malenka RC, Bear MF (2004). LTP and LTD: An embarrassment of riches. Neuron 44, 5–21.

Malenka RC, Nicoll RA (1999). Long-term potentiation—a decade of progress? Science 285, 1870–1874.

Maletic-Savatic M, Malinow R, Svoboda K (1999). Rapid dendritic morphogenesis in CA1 hippocampal dendrites induced by synaptic activity. Science 283, 1923–1927.

Matsuzaki M, Honkura N, Ellis-Davies GC, Kasai H (2004). Structural basis of long-term potentiation in single dendritic spines. Nature 429, 761–766.

McAnaney TB, Park ES, Hanson GT, Remington SJ, Boxer SG (2002). Green fluorescent protein variants as ratiometric dual emission pH sensors. 2. Excited-state dynamics. Biochemistry 41, 15489–15494.

Mott DD, Wasburn MS, Zhang S, Dingledine RJ (2003). Subunit-dependent modulation of kainate receptors by extracellular protons and polyamines. J Neurosci 23, 1179–1188.

Musleh W, Bi X, Tocco G, Yaghoubi S, Baudry M (1997). Glycine-induced long-term potentiation is associated with structural and functional modifications of alpha-amino-3-hydroxyl-5-methyl-4-isoxazolepropionic acid receptors. Proc Natl Acad Sci USA 94, 9451–9456.

Nachshen DA, Drapeau P (1988). The regulation of cytosolic pH in isolated presynaptic nerve terminals from rat brain. J Gen Physiol 91, 289–303.

Narahashi T, Moore JW, Scott WR (1964). Tetrodotoxin blockage of sodium conductance increase in lobster giant axon. J Gen Physiol 47, 965–974.
Nowak L, Bregestovski P, Ascher P, Herbert A, Prochiantz A (1984). Magnesium gates glutamate-activated channels in mouse central neurones. Nature 307, 462–465.
Onishi I, Lin PJ, Diering GH, Williams WP, Numata M (2007). RACK1 associates with NHE5 in focal adhesions and positively regulates the transporter activity. Cell Signal 19, 194–203.
Park M, Penick EC, Edwards JG, Kauer JA, Ehlers MD (2004). Recycling endosomes supply AMPA receptors for LTP. Science 305, 1972–1975.
Park M, Salgado JM, Ostroff L, Helton TD, Robinson CG, Harris KM, Ehlers MD (2006). Plasticity-induced growth of dendritic spines by exocytic trafficking from recycling endosomes. Neuron 52, 817–830.
Rocha MA, Crockett DP, Wong LY, Richardson JR, Sonsalla PK (2008). Na^+/H^+ exchanger inhibition modifies dopamine neurotransmission during normal and metabolic stress conditions. J Neurochem 106, 231–243.
Ronicke R, Schroder UH, Bohm K, Reymann KG (2009). The Na^+/H^+ exchanger modulates long-term potentiation in rat hippocampal slices. Naunyn Schmiedebergs Arch Pharmacol 379, 233–239.
Rotin D, Grinstein S (1989). Impaired cell volume regulation in Na^+/H^+ exchange-deficient mutants. Am J Physiol 257, C1158–65.
Sauvaigo S, Vigne P, Frelin C, Lazdunski M (1984). Identification of an amiloride sensitive Na^+/H^+ exchange system in brain synaptosomes. Brain Res 301, 371–374.
Shahi K, Marvizon JC, Baudry M (1993). High concentrations of glycine induce long-lasting changes in synaptic efficacy in rat hippocampal slices. Neurosci Lett 149, 185–188.
Shaner NC, Steinbach PA, Tsien RY (2005). A guide to choosing fluorescent proteins. Nat Methods 12, 905–909.
Shepherd JD, Huganir RL (2007). The cell biology of synaptic plasticity: AMPA receptor trafficking. Annu Rev Cell Dev Biol 23, 613–643.
Siesjo BK, von Hanwehr R, Nergelius G, Nevander G, Ingvar M (1985). Extra- and intracellular pH in the brain during seizures and in the recovery period following the arrest of seizure activity. J Cereb Blood Flow Metab 5, 47–57.
Smith GA, Brett CL, Church J (1998). Effects of noradrenaline on intracellular pH in acutely dissociated adult rat hippocampal CA1 neurones. J Physiol 512, 487–505.
Somjen GG (1984). Acidification of interstitial fluid in hippocampal formation caused by seizures and by spreading depression. Brain Res 311, 186–188.
Sutton MA, Wall NR, Aakalu GN, Schuman EM (2004). Regulation of dendritic protein synthesis by miniature synaptic events. Science 304, 1979–1983.
Sutton MA, Ito HT, Cressy P, Kempf C, Woo JC, Schuman EM (2006). Miniature neurotransmission stabilizes synaptic function via tonic suppression of local dendritic protein synthesis. Cell 125, 785–799.
Szaszi K, Paulsen A, Szabo EZ, Numata M, Grinstein S, Orlowski J (2002). Clathrin-mediated endocytosis and recycling of the neuron-specific Na^+/H^+ exchanger NHE5 isoform. regulation by phosphatidylinositol 3′-kinase and the actin cytoskeleton. J Biol Chem 277, 42623–42632.
Tang CM, Dichter M, Morad M (1990). Modulation of the *N*-methyl-D-aspartate channel by extracellular H^+. Proc Natl Acad Sci USA 87, 6445–6449.
Tombaugh GC, Somjen GG (1996). Effects of extracellular pH on voltage-gated Na^+, K^+ and Ca^{2+} currents in isolated rat CA1 neurons. J Physiol 493, 719–732.
Traynelis SF, Cull-Candy SG (1990). Proton inhibition of *N*-methyl-D-aspartate receptors in cerebellar neurons. Nature 345, 347–350.
Trudeau LE, Parpura V, Haydon PG (1999). Activation of neurotransmitter release in hippocampal nerve terminals during recovery from intracellular acidification. J Neurophysiol 81, 2627–2635.
Velisek L (1998). Extracellular acidosis and high levels of carbon dioxide suppress synaptic transmission and prevent the induction of long-term potentiation in the CA1 region of rat hippocampal slices. Hippocampus 8, 24–32.
Vilas GL, Johnson DE, Freund P, Casey JR (2009). Characterization of an epilepsy-associated variant of the human Cl^-/HCO_3^- exchanger AE3. Am J Physiol 297, C526–36.
Wang Z *et al*. (2008). Myosin Vb mobilizes recycling endosomes and AMPA receptors for postsynaptic plasticity. Cell 135, 535–548.
Xie C, Markesbery WR, Lovell MA (2000). Survival of hippocampal and cortical neurons in a mixture of MEM+ and B27-supplemented neurobasal medium. Free Radic Biol Med 28, 665–672.
Yaka R, Thornton C, Vagts AJ, Phamluong K, Bonci A, Ron D (2002). NMDA receptor function is regulated by the inhibitory scaffolding protein, RACK1. Proc Natl Acad Sci USA 99, 5710–5715.
Zha XM, Wemmie JA, Green SH, Welsh MJ (2006). Acid-sensing ion channel 1a is a postsynaptic proton receptor that affects the density of dendritic spines. Proc Natl Acad Sci USA 103, 16556–16561.